

1 **Social behavioral profiling by unsupervised deep learning reveals a** 2 **stimulative effect of dopamine D3 agonists on zebrafish sociality**

3
4 Yijie Geng*¹, Randall T. Peterson*¹

5
6 ¹Department of Pharmacology and Toxicology, College of Pharmacy, University of Utah, Salt Lake City,
7 UT 84112, USA

8 *Corresponding author: yijie.geng@pharm.utah.edu; randall.peterson@pharm.utah.edu

9 10 11 **ABSTRACT**

12 It has been a major challenge to systematically evaluate and compare how pharmacological perturbations
13 influence social behavioral outcomes. Although some pharmacological agents are known to alter social
14 behavior, precise description and quantification of such effects have proven difficult. The complexity of
15 brain functions regulating sociality makes it challenging to predict drug effects on social behavior without
16 testing in live animals, and most existing behavioral assays are low-throughput and provide only
17 unidimensional readouts of social function. To achieve richer characterization of drug effects on sociality,
18 we developed a scalable social behavioral assay for zebrafish named ZeChat based on unsupervised deep
19 learning. High-dimensional and dynamic social behavioral phenotypes are automatically classified using
20 this method. By screening a neuroactive compound library, we found that different classes of chemicals
21 evoke distinct patterns of social behavioral fingerprints. By examining these patterns, we discovered that
22 dopamine D3 agonists possess a social stimulative effect on zebrafish. The D3 agonists pramipexole,
23 piribedil, and 7-hydroxy-DPAT-HBr rescued social deficits in a valproic acid-induced zebrafish autism
24 model. The ZeChat platform provides a promising approach for dissecting the pharmacology of social
25 behavior and discovering novel social-modulatory compounds.

26

27

INTRODUCTION

28 Sociality is broadly conserved across the animal kingdom, facilitating cooperation, reproduction, and
29 protection from predation. In humans, social dysfunction is a hallmark of several neuropsychiatric disorders
30 such as autism, schizophrenia, bipolar disorder, and Williams syndrome, to name a few. In particular, social
31 communication impairment is considered a core symptom of autism. Despite its importance, we lack a
32 comprehensive understanding of how the diverse classes of neuroactive drugs impact social behavior. This
33 is evidenced by the fact that although certain antipsychotics, antidepressants, and stimulants medications
34 are used clinically to help manage some symptoms of autism^{1,2}, no treatment is currently available to
35 ameliorate the disease-relevant social deficit.

36 It has been a major challenge to comprehensively assess and compare how chemicals affect complex
37 behaviors such as sociality. Simple *in vitro* assays cannot effectively model drug effects on whole
38 organisms, especially on brain activity. Rodent models lack sufficient throughput and are cost-prohibitive
39 for a comprehensive examination of the hundreds of neuroactive drugs currently available, limiting their
40 uses to small-scale hypothesis-driven testing. On the other hand, the zebrafish has become an increasingly
41 important model organism for social behavioral research³, and recent developments in zebrafish behavioral
42 profiling have demonstrated a promising alternative approach to meeting this challenge. Indeed,
43 multidimensional behavioral profiling in zebrafish has been used to systematically assess thousands of
44 chemicals for effects on motor responses^{4,5}, rest/wake behavior⁶, and appetite⁷.

45 Current methods of social behavioral analysis in zebrafish are mostly limited to quantifying the average
46 measurement of a human-defined simplex trait such as social preference⁸, social orienting⁹, and group
47 cohesion¹⁰, or a collection of several simplex traits¹¹, with limited throughput. Restricted by their
48 unidimensional nature, these measurements often fail to adequately represent the complex and
49 multidimensional nature of social behavior in space and time. To comprehensively assess social behavior
50 for behavioral profiling, we sought to develop an automated method to classify the real-time dynamics of
51 social behavior based solely on information provided by the data, without any human intervention, in a
52 scalable format. To achieve this goal, we adopted an unsupervised deep learning approach: deep learning
53 based on a convolutional autoencoder can automatically extract social-relevant features from a behavioral
54 recording, while unsupervised learning allows for unbiased classification of real-time behavioral
55 phenotypes; both processes were conducted free of human instructions.

56 Here, we report a fully automated and scalable social behavioral profiling platform named ZeChat. Built
57 on an unsupervised deep learning backbone, ZeChat embeds the high-dimensional and dynamical social
58 behavioral data into a 2-dimensional space and assigns the embedded datapoints to distinct behavioral
59 categories, thus converting a fish's entire social behavioral recording to a behavioral fingerprint in the form
60 of a numerical vector. Screening 237 known neuroactive compounds using the ZeChat system generated a
61 rich set of social-relevant behavioral phenotypes which enabled unbiased clustering and classification of
62 drug-treated animals. Based on the social behavioral profile compiled from the screen, we discovered a
63 social stimulative effect of dopamine D3 receptor agonists (D3 agonists). Acute exposure to D3 agonists
64 rescued social deficits in a valproic acid-induced zebrafish autism model. Our results demonstrate that
65 multidimensional social behavioral phenotypes can be distilled into simple behavioral fingerprints to
66 classify the effect of psychotropic chemicals on sociality.

67

68

RESULTS

69 **Rationale and overview of the ZeChat behavioral analysis framework**

70 The ZeChat workflow is summarized in Figure 1a. We probed social interaction in a 2-chamber setup, in
71 which each fish swims freely in a square arena with visual access to its partner fish through a transparent
72 window. In this setup, a fish's position inside the arena, as well as its posture and movement dynamics,
73 were deemed relevant for social interaction. Inspired by Berman et al.¹², we sought to describe social
74 behavior as a point moving through a high-dimensional space of positional, postural, and motional features,
75 and to assign segmented subspaces to sub-behaviors. First, a preprocessing step distilled social-relevant
76 information from the recorded images. A convolutional autoencoder then unbiasedly extracted key features
77 from the preprocessed images to a latent vector, which is then projected onto its first 40 principal
78 components. We converted the time series of each principal component to a wavelet spectrogram to
79 incorporate behavioral dynamics into a feature vector. Finally, each feature vector was embedded into a 2-
80 dimensional map and classified to distinct behavioral categories.

81

82 **Social-relevant information can be extracted via behavioral recording and image preprocessing**

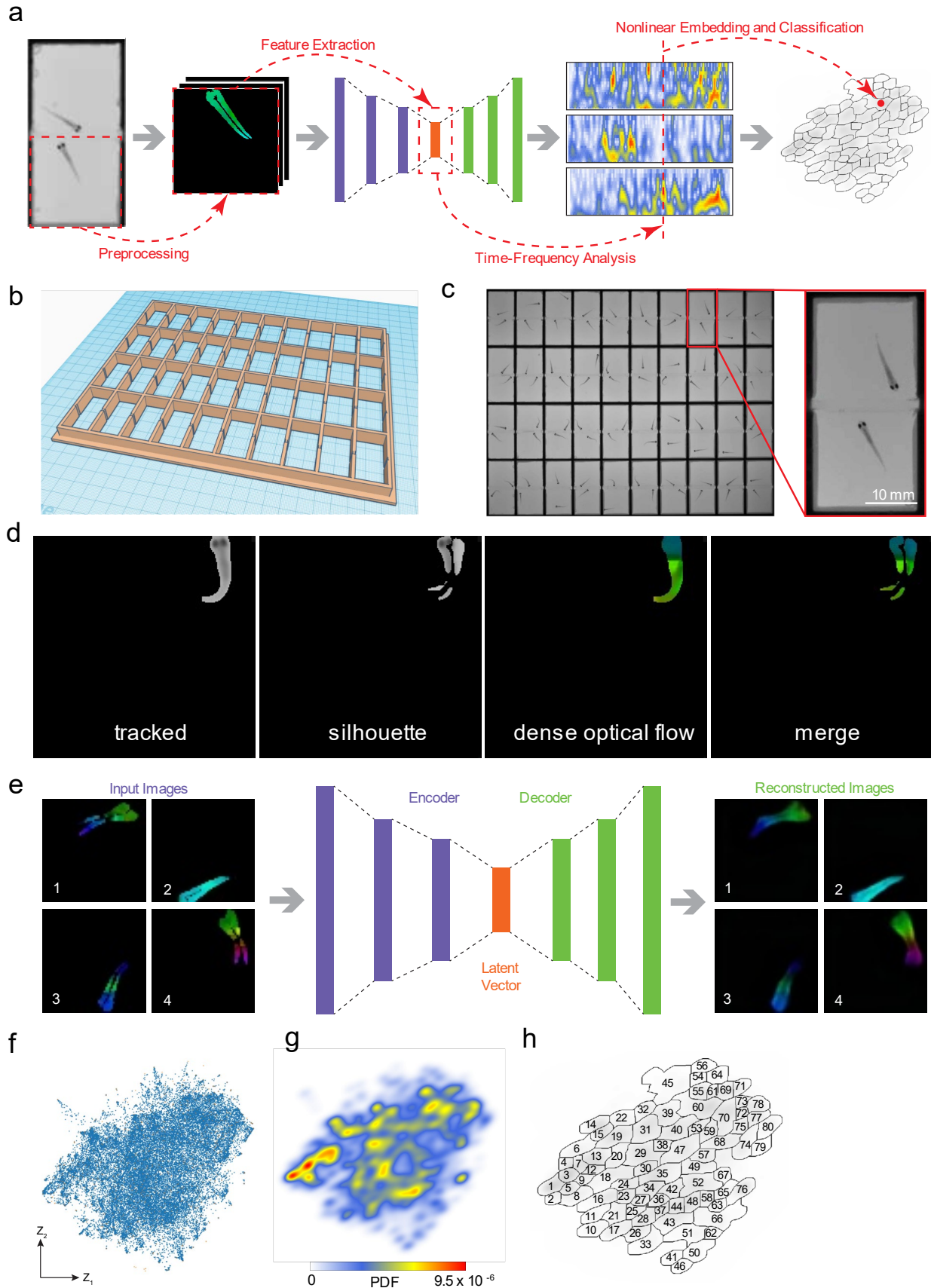
83 The zebrafish becomes socially active at 3 weeks of age⁸ while remaining small in size (~ 1 cm long),
84 enabling us to visualize social interaction in a confined space. To allow easy separation of individual fish
85 for subsequent analysis, pairs of fish were each placed in a separate 2 cm × 2 cm arena and allowed to
86 interact only through a transparent window (Supplementary Fig. 1a; Supplementary Video 1). A custom-
87 built high-throughput imaging platform was used to record 40 pairs of fish simultaneously with sufficient
88 spatiotemporal resolution to capture dynamic changes of the fish's postures and positions (Fig. 1b-c &
89 Supplementary Video 2). Sexual dimorphism is not readily apparent at this stage, so fish were paired
90 without sex distinction.

91 For image preprocessing, images of each arena were cropped with the transparent window always in the
92 upright position to preserve fish's positional information. Each fish was first tracked to be isolated from the
93 background (Fig. 1d & Supplementary Video 3: tracked). Consecutive frames were subtracted to show
94 postural changes between consecutive frames in the resulting silhouette (Fig. 1d & Supplementary Video
95 3: silhouette). In parallel, we colored each fish based on its instantaneous direction and velocity of
96 movement calculated by dense optical flow¹³ (Fig. 1d & Supplementary Video 3: dense optical flow).
97 Finally, each dense optical flow image was masked by its corresponding silhouette to generate a merged
98 image (Fig. 1c & Supplementary Video 3: merge; Supplementary Fig. 1c).

99

100 **Preprocessed images can be transformed to feature vectors by feature extraction and time-frequency** 101 **analysis**

102 Without any human intervention, convolutional autoencoders can automatically “learn” to extract useful
103 features from input images into a latent vector, which is then used to reconstruct these images. We therefore
104 used this deep learning architecture to extract key features of the preprocessed images into the latent vector
105 for subsequent analyses. As part of the initial setup, we first pre-trained the convolutional autoencoder using
106 a training set of preprocessed images (Fig. 1e & Supplementary Fig. 1d). The resulting latent vectors were
107 projected onto the first 40 principal components by a principal component analysis (PCA), preserving ~ 95%
108 of the total variance. When running the ZeChat analysis, preprocessed images were converted to time series
109 of 40 principal components by the pre-trained autoencoder and PCA models.



111 **Figure 1. The general framework of ZeChat behavioral analysis.** (a) To analyze a ZeChat recording, a separate video clip is
112 first generated for each fish by cropping out the ZeChat arena where it is located in. Each cropped video clip is orientated so that
113 the transparent window is always aligned to the top edge of the clip. Each frame is then Preprocessed to preserve positional,
114 postural, and motion related information. The preprocessed images are fed into an autoencoder for Feature Extraction. The main
115 principal components of the extracted feature vector are each converted to a spectrogram by Time-Frequency Analysis. The
116 resulting spectral feature vectors are embedded into a 2-dimensional map and classified to distinct behavioral categories by
117 Nonlinear Embedding and Classification. (b) The 3D design of the 40-unit ZeChat testing array. (c) A screenshot of ZeChat
118 recording. Also zoom in to show an independent testing unit. (d) Intermediate and resulting images of the preprocessing procedure.
119 Fish is first tracked to remove background (tracked). Consecutive tracked frames are subtracted (silhouette). In parallel, the tracked
120 fish is colored by dense optical flow (dense optical flow). Finally, the dense optical flow image is masked by the silhouette to
121 generate a merged image (merge). (e) Training the convolutional autoencoder. Preprocessed images (left, Input Images) are fed
122 into the 7-layer convolutional autoencoder (middle) to be reconstructed (right, Reconstructed Images). The Encoder layers are
123 responsible for compressing the input image into a latent representation space in the form of a Latent Vector, which is then used to
124 reconstruct the input image by the Decoder layers. (f) Training dataset embedded into a 2D ZeChat map. A reference map
125 containing 3000 datapoints (red) was first embedded using t-SNE. Kernel t-SNE was then used to embed an additional 60,000
126 datapoints (blue). (g) Probability density function (PDF) of ZeChat map containing 10,000 randomly selected datapoints. Generated
127 by convolving the ZeChat map with a Gaussian. (h) PDF of the ZeChat map was segmented into 80 distinct behavioral categories
128 by performing a watershed transform.

129 Behaviors happen in durations, necessitating time to be taken into consideration to properly interpret
130 information extracted from the behavioral recordings. To embed time-related information into the final
131 feature vector, we adopted the method of applying continuous wavelet transform (CWT) on the time series
132 of each of the 40 principal components to capture oscillations across many timescales¹². From the 40
133 resulting spectrograms, 25 amplitudes at each timepoint were concatenated into a single vector of length
134 40×25 . Up to this point, each original recorded frame was converted to a single 1,000-dimensional feature
135 vector (Supplementary Fig. 2).

136

137 **Feature vectors are assigned to behavioral categories by nonlinear embedding and classification**

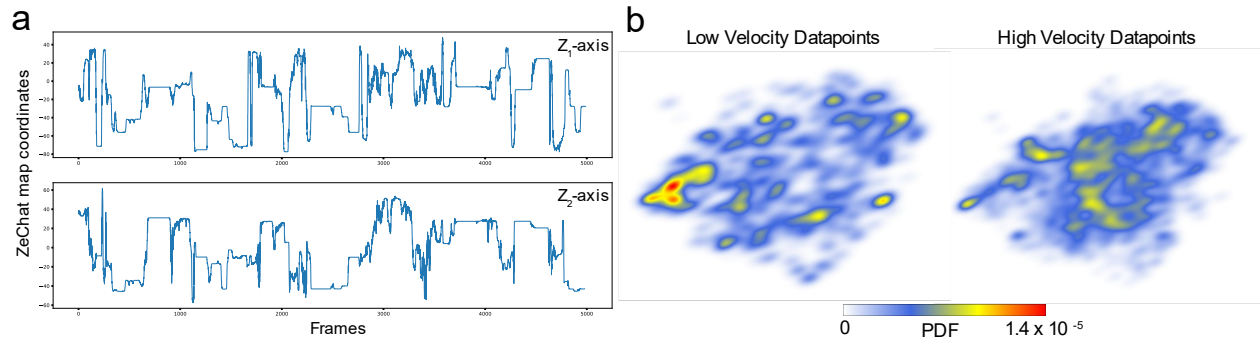
138 Finally, we adopted a method developed by Berman et al.¹², with modifications, to assign feature vectors
139 to behavioral categories through nonlinear embedding and classification. The high dimensional feature
140 vectors were embedded to a 2-dimensional space by nonlinear dimensionality reduction using *t*-distributed
141 stochastic neighbor embedding (*t*-SNE)¹⁴. Due to computational limitations, we first embedded a small
142 subset of randomly sampled feature vectors to create a reference map. Because *t*-SNE is non-parametric,
143 we applied a parametric variant of *t*-SNE named kernel *t*-SNE¹⁵ to embed additional datapoints onto the
144 reference map. We named the resulting 2-dimensional behavioral space ZeChat map (Fig. 1f).

145 Calculating the probability density function (PDF) of ZeChat map identified regions with high datapoint
146 density as local maxima (Fig. 1g), marking the locations of potential behavioral categories¹². We segmented
147 ZeChat map into 80 regions based on locations of the local maxima using a watershed transform algorithm,
148 allowing each original recorded frame – now embedded as a datapoint in ZeChat map – to be assigned to a
149 particular behavioral category (Fig. 1h).

150

151 **The pause-move dynamic of ZeChat map**

152 We made videos to help visualize how a fish's real-time behavioral changes translate to datapoint
153 trajectories on the ZeChat map (Supplementary Video 4). We found that the trajectory of the 2-dimensional
154 embedding alternates between sustained pauses within certain regions of the map and rapid movements
155 from one region to a distant region on the map. Plotting the velocity of the trajectory revealed a “pause-
156 move” dynamic (Fig. 2a). The low-velocity points were localized in distinguishable peaks that often
157 overlapped with the ZeChat map's local maxima (Fig. 2b & 1g). In contrast, the high-velocity points were
158 more uniformly distributed (Fig. 2b). This result supports the idea that the social-relevant behavioral
159 changes can be represented by a course through a high-dimensional space of postural, motional, and
160 positional features in which the course halts at locations that correspond to discrete sub-behaviors¹².



162 **Figure 2. The pause-move dynamic of ZeChat map.** (a) A typical datapoint trajectory in the Z_1 and Z_2 axes of ZeChat map.
163 Showing a pause-move dynamic. (b) PDF maps of low velocity (< 1) and high velocity (≥ 1) datapoints. Local maxima positions
164 of the low velocity PDF map closely match local maxima positions in Fig. 2g, whereas the high velocity datapoints showed a more
165 uniform distribution pattern.

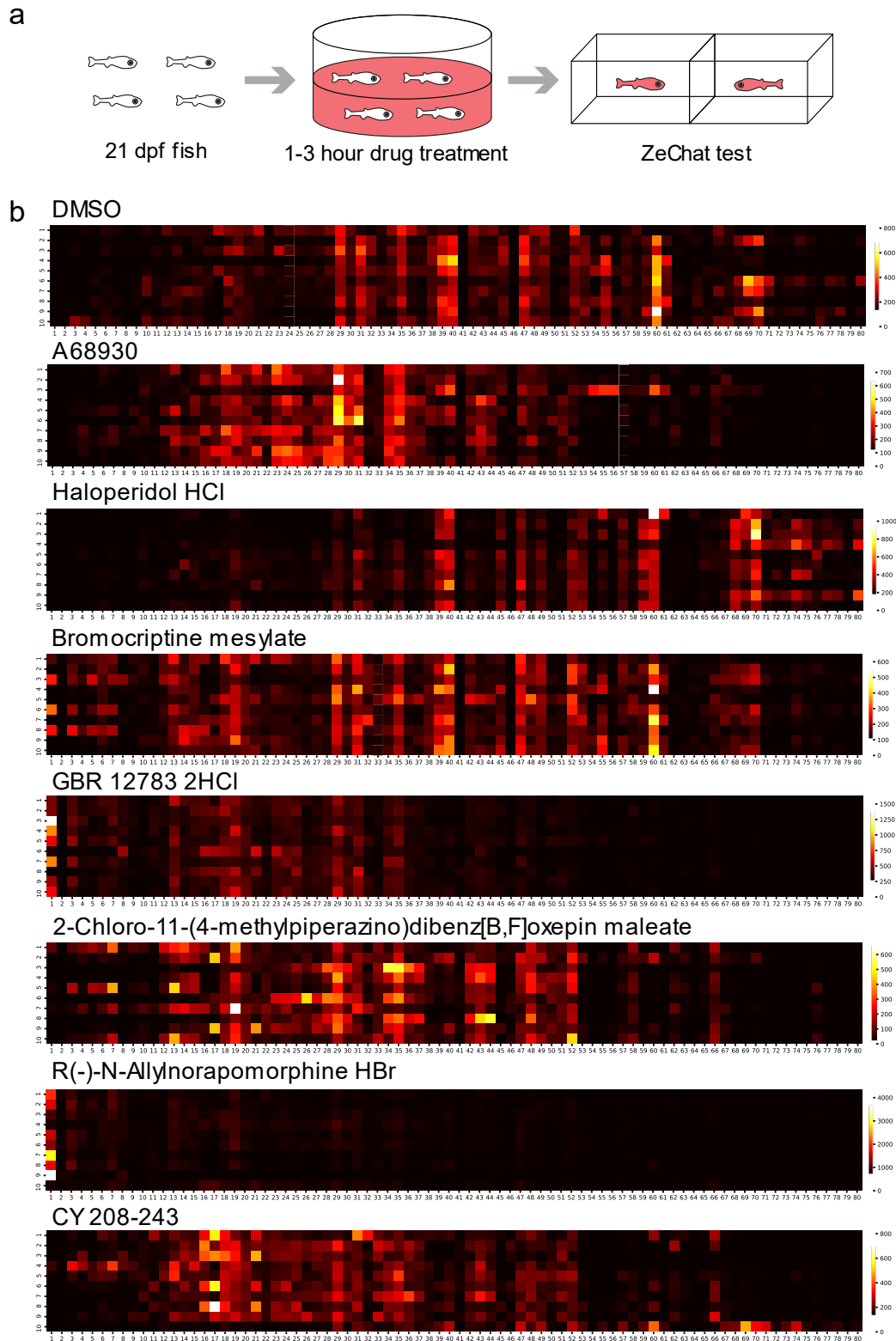
166

167 Neuroactive compound screening reveals diverse social behavioral responses

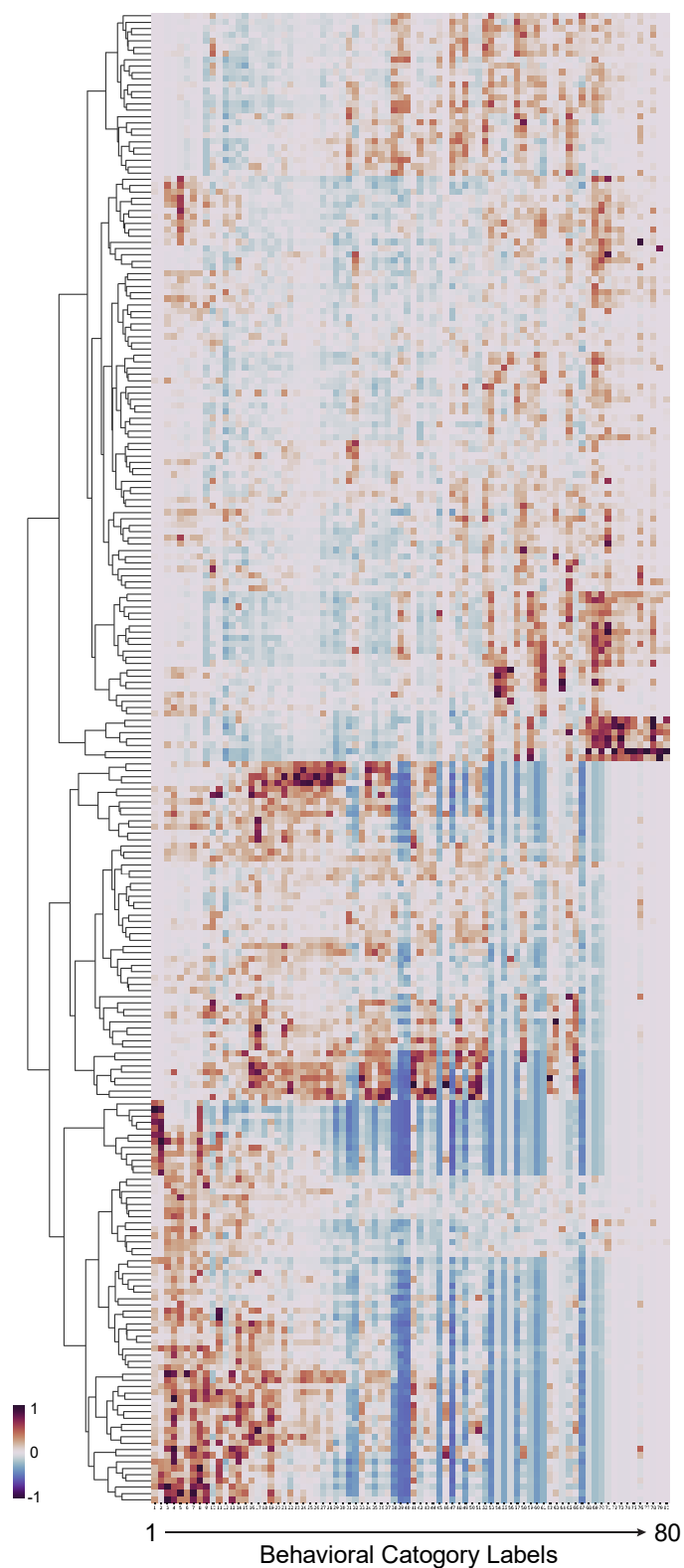
168 To systematically assess how neuroactive compounds modulate social behavior, we conducted a screen of
169 237 compounds including modulators of the dopamine, serotonin, and opioid-related pathways. These
170 pathways were selected because they have been implicating in influencing social behavior¹⁶⁻¹⁸. Briefly, 3-
171 week-old juvenile fish were treated with compounds by bath exposure for 1-3 hours prior to ZeChat
172 recording. Ten fish were treated with each compound, and fish treated with the same compound were paired
173 with each other for ZeChat recording (Fig. 3a). A set of DMSO control fish was included in every recording.

174 Counting the number of times a fish's behavior is classified to each behavioral category generated a
175 behavioral fingerprint in the form of an 80-dimensional numerical vector. Fish treated with the same
176 compound showed highly similar behavioral fingerprints (Fig. 3b), suggesting that the behavioral
177 fingerprints produced by a given compound are consistent across multiple individual animals. To
178 consolidate data, we combined the behavioral fingerprints of fish treated with the same compound by
179 keeping the median value of each behavioral category. All 237 consolidated behavioral fingerprints plus
180 DMSO controls were normalized, and the medians of DMSO controls were subtracted from all samples to
181 help visualize changes in behavioral fingerprints compared to wild type behavior.

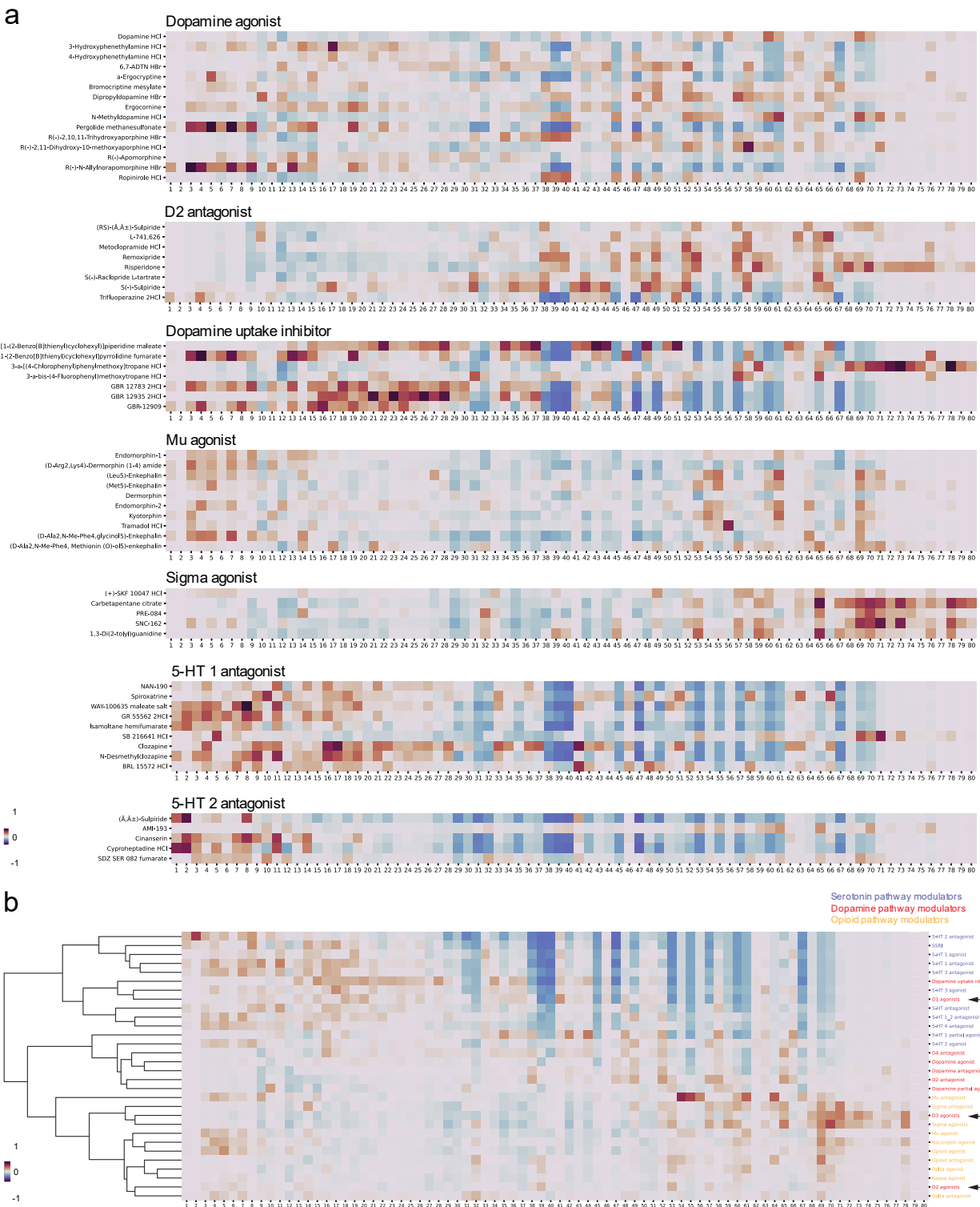
182 Hierarchical clustering reveals a diversity of behavioral responses (Fig. 4 & Supplementary Fig. 3). We
183 found that compounds belonging to the same functional class consistently evoked highly similar behavioral
184 fingerprints (Fig. 5a and Supplementary Fig. 4 & 5). To compare the typical behavioral fingerprints of
185 major drug classes, we calculated the median value of each behavioral category for all behavioral
186 fingerprints elicited by functionally similar molecules. Only drug classes with no fewer than 3 compounds
187 tested in the screen were included in this analysis. Hierarchical clustering of the resulting behavioral
188 fingerprints again revealed distinct behavioral phenotypes (Fig. 5b). Remarkably, compounds targeting the
189 3 major neurotransmitter pathways, e.g., the serotonin, dopamine, and opioid pathways, were naturally
190 separated by hierarchical clustering (Fig. 5b: functional classes of drugs are color coded to distinguish the
191 3 major pathways).



193 **Figure 3. Neuroactive compounds produce highly reproducible behavioral fingerprints.** (a) A schematic of the screening
194 procedure. (b) Behavioral fingerprints of individual fish treated by different chemicals. Each row represents the behavior fingerprint
195 of an individual fish. Each square represents the total number of times a fish is assigned to a behavioral category. Horizontal axis:
196 the 80 behavioral categories. Color bar: cumulated number of times a fish is assigned to a behavioral category.



198 **Figure 4. Hierarchical clustering reveals distinct drug-induced behavioral responses.** Hierarchical clustering of behavioral
199 fingerprints generated by the screen. Each behavioral fingerprint (row) represents the median value of the individual fingerprints
200 of all fish ($n \leq 10$ per treatment) treated by the same compound. The behavioral fingerprints are normalized for each behavioral
201 category and subtracted by the median DMSO fingerprint. Horizontal axis labels the 80 behavioral categories.

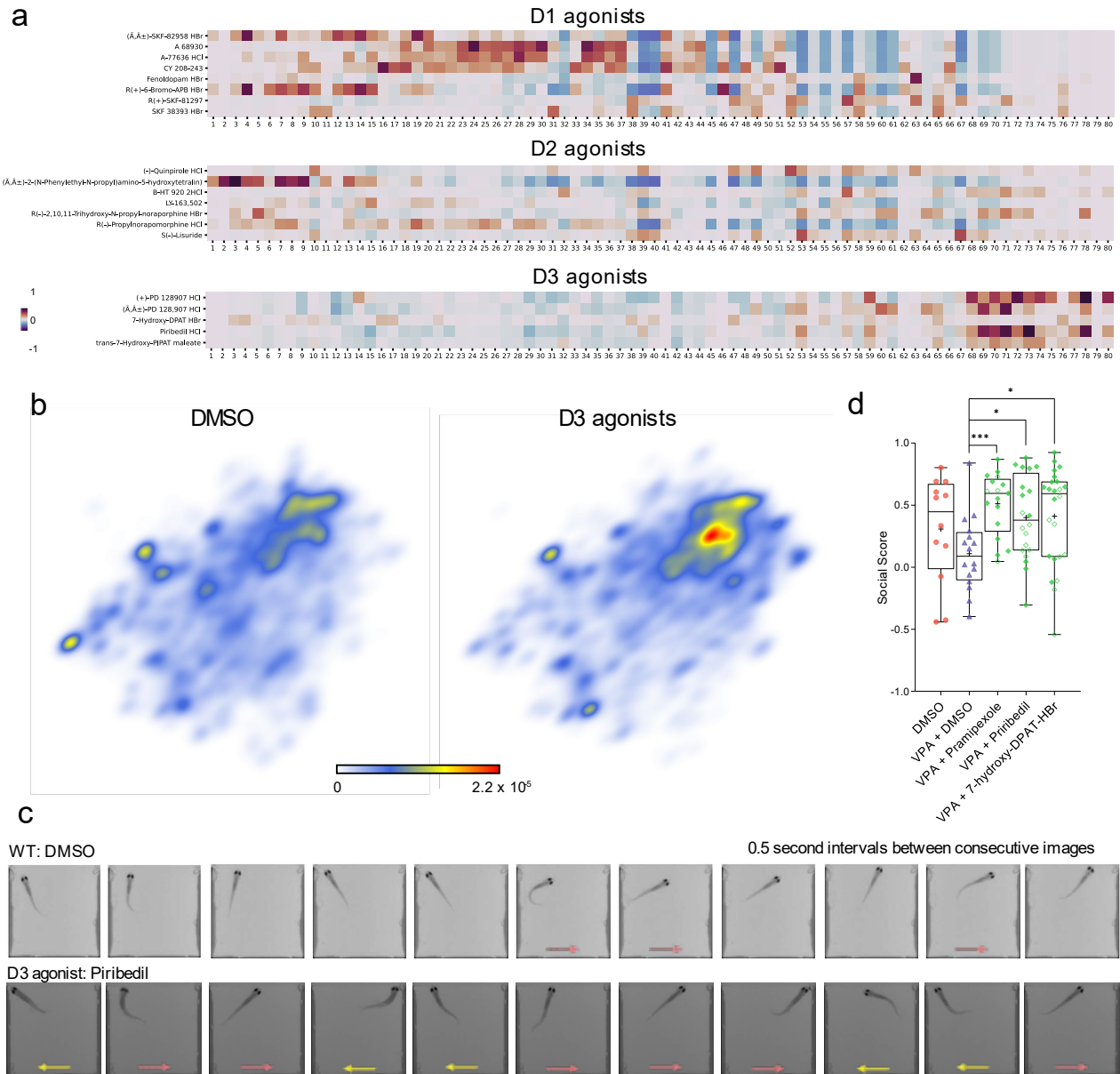


203 **Figure 5. Functionally similar molecules evoke similar behavioral responses.** (a) Neuroactive compounds with similar
 204 annotated functions elicit similar behavioral fingerprints. (b) Behavioral fingerprints of functionally similar molecules are
 205 consolidated to a single behavioral fingerprint by calculating the median value of each behavioral category, and the resulting
 206 behavior fingerprints are hierarchically clustered. Only groups of drugs containing no less than 3 compounds sharing the same
 207 annotated function are included in the analysis. The group labels are colored by the targeted pathway. Black arrows point to
 208 behavioral fingerprints of dopamine D1, D2, and D3 receptor agonists, respectively.

209 **Dopamine D3 receptor agonists rescue social deficits in a VPA-induced autism model**

210 Surprisingly, we noticed that the dopamine D1, D2, and D3 receptor agonists were clustered well apart
211 from each other (Fig. 5b: black arrows), suggesting that selected activations of the dopamine D1, D2, and
212 D3 receptor-related neuronal circuits elicited distinct social behavioral phenotypes. The five D3 agonists
213 tested in the 237-compound screen generated highly similar behavioral fingerprints sharing a unique pattern
214 in which strong signals are observed in the higher-number behavioral categories (Fig. 6a-b). In contrast, the
215 D1 and D2 agonists elicited very different behavioral fingerprints with no enrichment in these higher-
216 number behavioral categories (Fig. 6a). By examining raw behavioral recordings, we noticed that the D3-
217 agonist-treated fish tend to spend a significant amount of time swimming intensively while pressing against
218 the transparent window. Compared to wild type animals, these fish demonstrated persistent and strong high-
219 frequency tail beats, fast swim velocity, and quick and frequent turns; they also rarely retreated from
220 proximity to the transparent window (Supplementary Video 5 and Fig. 6c). We hypothesized that these D3
221 agonist-associated behaviors may signify enhanced sociality.

222 We attempted to validate the hypothesized social stimulative property of D3 agonists in a zebrafish autism
223 model with a social deficit phenotype. Embryonic exposure to valproic acid (VPA) is an established model
224 of autism in rodents¹⁹ and zebrafish²⁰. Using a simple zebrafish social preference assay²¹, we observed a
225 clear social deficit phenotype in VPA-treated zebrafish (Supplementary Fig. 6a). To test the effect of D3
226 agonists against social deficits, we acquired 3 structurally diverse D3 agonists, pramipexole, piribedil, and
227 7-hydroxy-DPAT-HBr (Supplementary Fig. 6b). Both pramipexole and piribedil are FDA-approved
228 antiparkinsonian agents. We found that exposure to D3 agonists for 1 hour by simple submersion prior to
229 the social preference assay effectively rescued the social deficit in the VPA-treated fish (Fig. 6d).



231 **Figure 6. Dopamine D3 agonists rescue social deficits in VPA-treated fish.** (a) Comparing the behavioral fingerprints of D1,
 232 D2, and D3 agonists. The behavioral fingerprints are normalized and subtracted by the median DMSO fingerprint. (b) PDF maps
 233 of DMSO-treated fish (n=356) and fish treated by D3 agonists (n=49). (c) Series of images taken at 0.5 second intervals reveal
 234 different swim dynamics between wild type treated by DMSO and fish treated by the D3 agonist piribedil (10 μ M). Arrows in red
 235 and yellow point to fish's direction of movement in the current frame. (d) Boxplot showing social preference (social score) of
 236 DMSO-treated fish (n=12) or VPA-treated fish acutely exposed to DMSO (n=16) or 10 μ M D3 agonist including pramipexole
 237 (n=17), piribedil (n=20), and 7-hydroxy-DPAT-HBr (n=24) for 1 hour before social preference test. In each boxplot, box encloses
 238 data points from the 25th percentile to the 75th percentile, the horizontal line and cross mark the median and the mean, the lines
 239 above and below the box reach datapoints with the maximum and minimum values. *: $p < 0.05$, ***: $p < 0.001$.

241

DISCUSSION

242 ZeChat is a deep learning-based behavioral assessment tool enabling scalable and low-cost zebrafish
243 behavioral profiling to characterize changes in sociality. The *in vivo* ZeChat platform combines advantages
244 of *in vitro* and rodent models, enabling scalable testing with high behavioral resolution. Compared to
245 previous zebrafish behavioral profiling methods, the ZeChat analysis method specifically processes and
246 analyzes social behavior-relevant information, linking known neuroactive drugs with complex but distinct
247 social behavioral outcomes.

248 Apart from unsupervised machine learning, alternative approaches are available for improving the
249 resolution of social behavioral analysis, but not without drawbacks. For example, supervised machine
250 learning methods have been widely adopted to analyze social interactions in fruit fly^{22,23}, zebrafish²⁴, and
251 mouse²⁵. However, this method still relies on human interpretation of animal behavior to classify and assign
252 behavior and is likely unable to fully reveal the complexity and subtlety of social behavior. Another
253 approach uses predefined measurement criteria to mathematically model and classify social interaction^{26,27},
254 which reduces human biases in the analysis, but the quality of its outcome is highly dependent upon the
255 validity of the model. In comparison, unsupervised methods have successfully revealed stereotypic
256 behavioral motifs in individual animals of *C. elegans*²⁸⁻³⁴, fruit fly^{12,35-39}, zebrafish⁴⁰⁻⁴², and mouse^{43,44}, as
257 well as paired interactions in fruit fly^{45,46}, without any human interventions or *a priori* assumptions,
258 providing a viable approach for our purpose.

259 However, all these approaches still rely on manual selection of features for data preprocessing, which
260 requires strong domain knowledge in the behaving animal. These prerequisites are not always met,
261 especially when faced with complex problems such as analyzing subtle behavioral changes in a video or
262 analyzing sequences of behaviors, as it is difficult for a human observer to exhaustively extract useful
263 features from an image or a sequence of images. Deep learning methods, on the other hand, can
264 automatically learn to extract abstract features from images. As behavioral recordings are sequences of
265 images, the potential benefit for applying deep learning to process these data is apparent. In fact, several
266 recent studies have successfully utilized deep learning to facilitate individual animal identification⁴⁷,
267 tracking⁴⁸, and movement prediction⁴⁹ in zebrafish, paving the way for its application in ZeChat.

268 In alignment with our findings, the D3 receptor has been previously implicated in social behavioral
269 regulation. In humans, pramipexole alleviates social anxiety in selective serotonin reuptake inhibitor
270 (SSRI)-treated patients⁵⁰. In rodents, two D3 agonists 7-OH-DPAT and PD 128907 were reported to cause
271 a variety of complex alterations in social behavior^{51,52}. Further investigations are needed to validate these
272 findings in rodents using other D3 agonists and under different test conditions, drug doses, and genetic
273 backgrounds of the animals, but the results in zebrafish, rats, and humans all point to an important role of
274 D3 receptors in modulating social behavior. In addition, because both pramipexole and piribedil are FDA-
275 approved antiparkinsonian agents, it may be worthwhile examining their impact on the social behavior of
276 patients receiving these drugs.

277 Future studies using the ZeChat platform may expand to screening other neuroactive compounds,
278 compounds with no known neuroactivity, and uncharacterized compounds, in the hope of identifying
279 additional phenotypes and drug classes with social-modulatory properties. The characteristic behavioral
280 fingerprint of the D3 agonists may be used to discover novel compounds with similar behavioral effects. In
281 addition to wild type fish, fish carrying mutations relevant to human psychiatric disorders can also be
282 assayed, and their behavioral fingerprints compared to the neuroactive compound clustergram to associate
283 genetic mutations with perturbations of neuronal pathways. As demonstrated by Hoffman et al.⁵³, small
284 molecules evoking an anti-correlated behavioral fingerprint may ameliorate social deficits in the mutant
285 fish. Hence, by providing a rapid, high-resolution means of characterizing and categorizing zebrafish with
286 altered social behaviors, ZeChat represents a useful tool for investigating the role of genes and
287 pharmacological agents in modulating complex social behaviors.

288

MATERIALS AND METHODS

289 **The ZeChat imaging system setup**

290 The basic unit of this system is a 10 mm deep, 20 mm wide, and 41.5 mm long (internal dimension)
291 rectangular chamber with 2 mm thick walls. A 10×4 array consist of 40 independent testing units was 3D
292 printed using white PLA at 100% infill. The printed test arena was glued onto a 3/16" thick white translucent
293 (43% light transmission) acrylic sheet (US Plastic) using a silicone sealer (Marineland). Each unit was then
294 divided into two square-shaped compartments by inserting a 1.5 mm thick transparent acrylic window –
295 precision cut to 10 mm x 41 mm pieces using a laser cutter – into 0.5 mm deep printed slots located in the
296 middle of each unit on the side of the 41.5 mm wall and fastened using the silicone sealer.

297 The key component of the imaging system is a 322 mm diameter bi-telecentric lens (Opto Engineering)
298 with an IR (850 nm) bandpass filter (Opto Engineering). A telecentric lens only allows passing of light that
299 is parallel to the optical axis, thus avoiding parallax error in imaging, and enables all test units – being
300 located either in the middle or close to the edge of the field of view – to be imaged without distortion.
301 Videos were taken at 50 frames per second (fps) by a 75 FPS Blackfly S Mono 5.0 MP USB3 Vision camera
302 (PointGrey) with a resolution of 2448 x 2048. The tail beat frequency (TBF) for adult zebrafish is ~ 20 Hz⁵⁴,
303 therefore images taken at 50 Hz by the camera should adequately sample motion-relevant features based
304 on the Nyquist–Shannon sampling theorem. The imaging platform was back-illuminated with an infrared
305 (850 nm) LED array (EnvironmentalLights) to provide light for video recording. The infrared LED array
306 was positioned on top of a heat sink (H S Marston). The imaging platform was also illuminated from two
307 opposing sides using white LED arrays (EnvironmentalLights) to provide ambient light for the test subjects.
308 Structural supports and enclosure were custom built using parts purchased from Thorlabs, McMaster Carr,
309 and US Plastic.

310

311 **ZeChat test**

312 Test subjects were individually placed into each unit – one on each side of the transparent window – using
313 a transfer pipette with its tip cut off. Their visual access to each other was temporarily blocked by a 3-D
314 printed nontransparent comb-like structure (Supplementary Fig. 1b) prior to each recording session. Once
315 all test subjects were placed into test arenas, the entire test apparatus was transferred into the imaging station
316 and the combs were removed to allow visual access between each pair of fish.

317 The 2-compartment social interaction setup allows the behavior of each fish to be recorded and analyzed
318 independently without having to go through complex and often computationally demanding and time-
319 consuming tracking procedures to separate each fish. Videos were streamed and recorded using the software
320 Bonsai⁵⁵. A 10 min test session was video recorded for each test. To give fish an acclimation period at the
321 beginning of each test and to take into consideration that the effects of some of the drugs tend to wear off
322 quickly, only the 5 min video segment between 2.5 min and 7.5 min was used for subsequent analyses. All
323 subsequent data processing and analyses were conducted in Python using packages including OpenCV,
324 scikit-learn, Keras, PyWavelets, and imutils.

325

326 **Data preprocessing**

327 For data preprocessing, individual fish were first separated from the background using the K-nearest
328 neighbors method⁵⁶. A separate video segment was cropped out for each fish which contains a recording of
329 the entire square compartment where the fish is located. Because the relative position of a fish to its
330 compartment is relevant to social interaction dynamics, each compartment was analyzed as a whole. And
331 because each compartment is polarized, with only one of the four sides being transparent to another fish,
332 for each pair of compartments, the video containing fish in the “top” compartment is flipped vertically by
333 rotating 180 degrees to match the orientation of video recording the “bottom” compartment, so that the side

334 of the compartment facing the transparent widow always faces upward in each video.

335 To capture changes in each fish's posture between consecutive frames, we subtracted every current frame
336 from its previous frame. The resulting images were binary-thresholded to generate silhouette-like masks.
337 In parallel, we calculated each fish's direction of movement between consecutive frames using the
338 Franeback Method of dense optical flow¹³ and used this information to color the fish; motionless fish appear
339 dark after applying this method, thus restricting our analysis to fish in motion. Finally, we applied the mask
340 acquired by subtracting consecutive frames to the dense optical flow image so that the image colored by
341 dense optical flow is cropped by the subtracted silhouette-like mask.

342

343 **Training the convolutional autoencoder and feature extraction**

344 The architecture of the convolutional autoencoder consists of three encoding layers each containing 64, 32,
345 and 16 filters, and three decoding layers each containing 16, 32, and 64 filters. We used a training set of
346 preprocessed images to pre-train the convolutional autoencoder. The preprocessed images with a dimension
347 of 220 pixels \times 220 pixels were first resized to 56 pixels \times 56 pixels to reduce computational requirements.
348 Because a wild type fish typically spends most of the time interacting with its paired fish by staying close
349 to the transparent window, causing the position of the fish in input images to be highly polarized, we
350 enriched the training dataset by rotating each resized image by 90°, 180°, and 270° to generate input images
351 with more postural and positional variations.

352 The autoencoder forces input images to pass through a “bottleneck” before reconstruction. The bottleneck,
353 or the latent representation space, has a dimension of 784. We then applied principal component analysis
354 (PCA) to this 784-dimensional feature vector and extracted 40 principal components which preserved ~ 95%
355 of total variance.

356

357 **Time-frequency analysis of feature dynamics**

358 Calculating the 40 principal components for each video frame yields 40 timeseries for each video. Each
359 timeseries was then expanded into a spectrogram by applying the Continuous Wavelet Transform (CWT).
360 The Morlet wavelet was used as the mother wavelet and 25 scales were chosen to match frequencies
361 spanning from 0.38 Hz to 5 Hz, with the range of frequencies empirically determined to preserve the
362 strongest signals. The time-frequency representation augments the instantaneous representation by
363 capturing oscillations across many timescales. The spectral amplitudes of each time point were then
364 concatenated into a vector of length 40 \times 25, giving rise to a 1,000-dimensional representation for each
365 original video frame. Each 1,000-dimensional vector was normalized to having a sum of 1 in order to treat
366 each vector as a probability distribution for subsequent calculation.

367

368 **Nonlinear embedding and segmentation**

369 We then performed nonlinear dimensionality reduction on these high dimensional vectors using the popular
370 nonlinear manifold embedding algorithm *t*-distributed stochastic neighbor embedding (*t*-SNE)¹⁴. We
371 randomly selected and embedded 3,000 feature vectors from 60 fish to generate a reference map. The *t*-
372 SNE algorithm is non-parametric. Therefore, additional datapoints were embedded onto the reference map
373 using a parametric kernel *t*-SNE¹⁵ method to form the ZeChat map. As the feature vectors are normalized
374 and treated as probability distributions, we calculated the Jensen–Shannon distance (the square root of the
375 Jensen–Shannon divergence) between each pair of vectors as a distance metric for both *t*-SNE and kernel
376 *t*-SNE. We chose the Jensen–Shannon distance as a metric for calculating distances due to it being
377 symmetric and bounded by 0 and 1 which avoids the generation of infinite values.

378 We calculated the probability density function (PDF) of this map by convolving with a Gaussian kernel.

379 Due to computational limitations, this calculation was conducted using a ZeChat map containing 10,000
380 randomly selected datapoints. The resulting probability density map was then inverted to turn local maxima
381 into “valleys”. The “ridges” between valleys were detected using Laplacian transform. Finally, a watershed
382 transform was applied to mark the borders between each valley to unbiasedly segment the ZeChat map into
383 80 behavioral categories.

384 For ZeChat analysis, to reduce computation time, we randomly sampled 5000 frames from each fish for
385 kernel *t*-SNE embedding and subsequent analyses.

386

387 **Behavioral fingerprint calculation and hierarchical clustering**

388 Each frame is assigned a watershed region (behavioral category) based on ZeChat map segmentation. For
389 each fish, the total number of frames assigned to each watershed region was counted, giving rise to a
390 behavioral fingerprint in the form of an 80-dimensional vector. Behavioral fingerprints of fish treated by
391 each drug were combined into one fingerprint by calculating the median of each behavioral category. All
392 combined raw behavioral fingerprints were normalized so that the signals of each behavioral category were
393 between 0 and 1. To help visualize the difference in behavioral patterns between drug treatments and DMSO
394 control, we calculated the median of each behavioral category of all DMSO controls to generate a
395 representative fingerprint for DMSO control, and subtracted this fingerprint from all drug treatment samples.
396 Finally, the normalized and DMSO-subtracted fingerprints of each drug treatment were clustered using the
397 clustermap function (metric='euclidean', method='complete') of Python's Seaborn library.

398

399 **Zebrafish chemical treatment and screening**

400 For ZeChat testing, 21 dpf zebrafish were collected from nursery tanks. Fish of roughly average size were
401 selected to minimize the effect of size differences. For the screen, 10 fish were picked into a 60 mm petri
402 dish containing 10 ml E3 medium. Compounds were then added to each dish at a final concentration of 10
403 μ M (non-peptide molecules) or 1 μ M (endogenous neuropeptides and their analogs). Fish were incubated
404 for 1-3 hours prior to ZeChat testing. Immediately before testing fish in a petri dish, the content of the petri
405 dish was poured through a nylon tea strainer to remove liquid while keeping fish in the tea strainer. The tea
406 strainer was then consecutively dipped into 3 petri dishes containing E3 to wash the residual chemical away
407 from the fish. The fish were then poured into a petri dish containing clean E3 and each individual was
408 transferred into the ZeChat test arena using a plastic transfer pipette for testing.

409

410 **Rescue of VPA fish and social preference testing**

411 VPA treatment was conducted by submerging embryos in 1 μ M VPA in E3 medium from 0 to 3 dpf. The
412 drug treated embryos were washed at 3 dpf and transferred to petri dishes containing clean E3 medium. At
413 5-7 dpf, larvae were transferred into nursery tanks and raised to 21 dpf for behavioral testing of social
414 preference using a 3-chamber assay apparatus²¹. For the D3 agonist rescue experiment, 20 VPA-treated fish
415 were picked into a 25 mm deep 10 cm petri dish containing 30 ml E3 medium. Compounds were then added
416 to each dish and fish were incubated for 1 hour. Immediately before testing, fish were washed as described
417 above, and individually placed into the social preference testing arenas for behavioral testing.

418

419 **Chemical library and other compounds**

420 All screening compounds were acquired from the Biomol neuroactive compound library (Biomol) which
421 contains a total of 700 neuroactive drugs dissolved in DMSO at a stock concentration of 10 mM or 1 mM
422 (for only a small subset of drugs). Valproic acid was purchased from Sigma-Aldrich. Pramipexole was
423 purchased from Cayman Chemical. Piribedil was purchased from Selleck Chemicals. 7-hydroxy-DPAT-

424 HBr was purchased from Santa Cruz. All individually purchased compounds were dissolved in DMSO.
425 Chemical structures were generated using PubChem Sketcher.

426

427 **Zebrafish husbandry**

428 Fertilized eggs (up to 10,000 embryos per day) were collected from group mating of EkkWill strain
429 zebrafish (*Danio rerio*) (EkkWill Waterlife Resources). Embryos were raised in HEPES (10 mM) buffered
430 E3 medium at 28°C, with or without compound treatment, during the first 3 days. At 3 days post fertilization
431 (dpf), chorion debris was removed, and larvae were transferred into petri dishes containing fresh E3 medium.
432 At 5 – 7 dpf, larvae were transferred into nursery tanks and raised at 28°C on a 14/10 hr on/off light cycle.

433

434 **Statistical analysis**

435 Graphs were generated using GraphPad Prism or Python using the Matplotlib package. Data were analyzed
436 using the 2-tailed Student's *t*-test. P values less than 0.05 were considered significant.

437

438 **Code availability**

439 Code is available on the GitHub repository at <https://github.com/yijie-geng/ZeChat> and is archived on
440 Zenodo under DOI: 10.5281/zenodo.5519964.

441

442

443

AUTHOR CONTRIBUTIONS

444 Y.G. conceived the study, built the equipment, designed and conducted the experiments, wrote the Python
445 codes, analyzed the data, and wrote the manuscript. R.T.P conceived the study, designed the experiments,
446 interpreted the data, and revised the manuscript.

447

448

ACKNOWLEDGEMENTS

449 We thank members of our research group for helpful advice. This work was supported by the L. S. Skaggs
450 Presidential Endowed Chair and by the National Institute of Environmental Health Sciences of the National
451 Institutes of Health under Award Number K99ES031050. The content is solely the responsibility of the
452 authors and does not necessarily represent the official views of the National Institutes of Health.

453

454

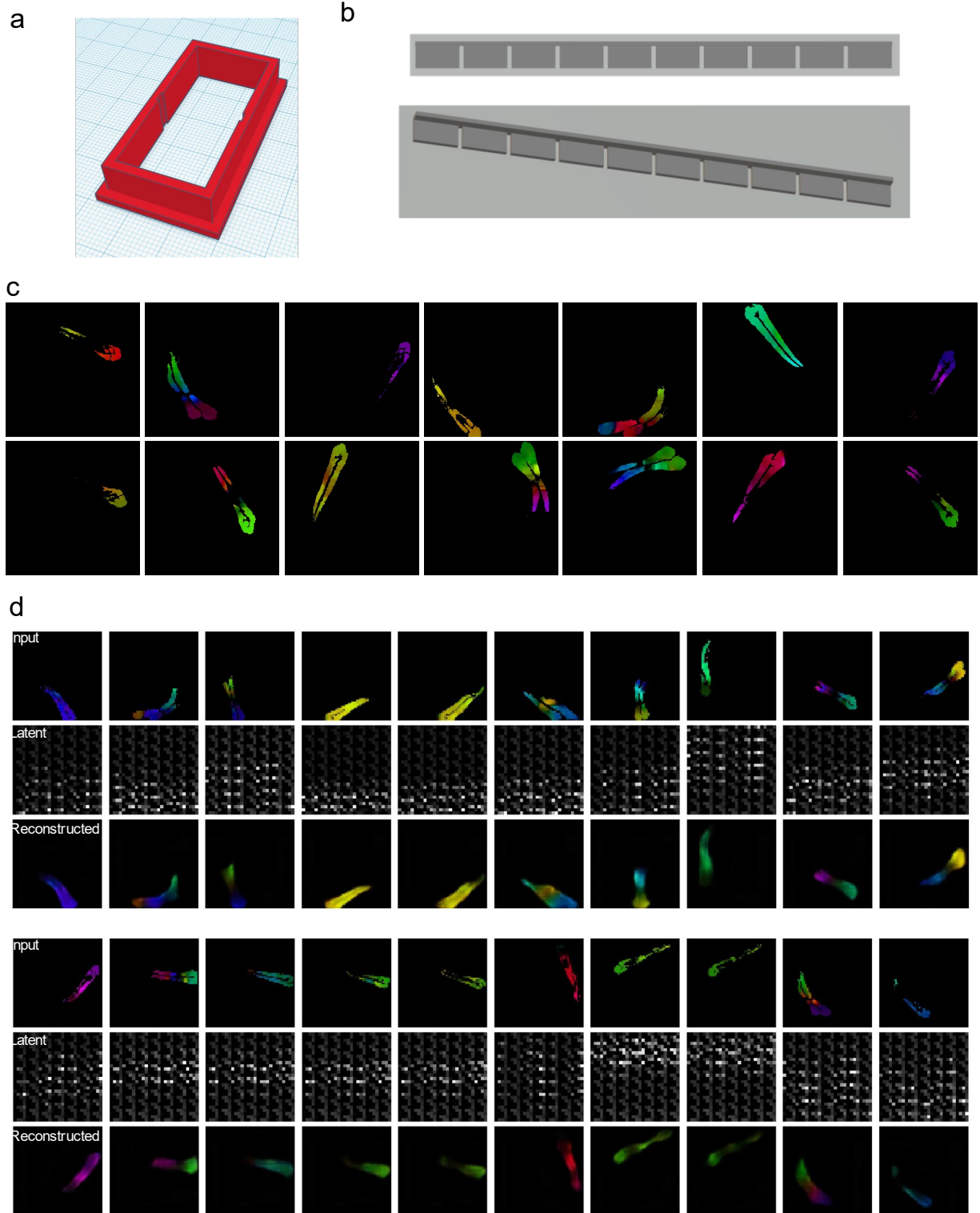
COMPETING INTERESTS

455 The authors declare no competing interests.

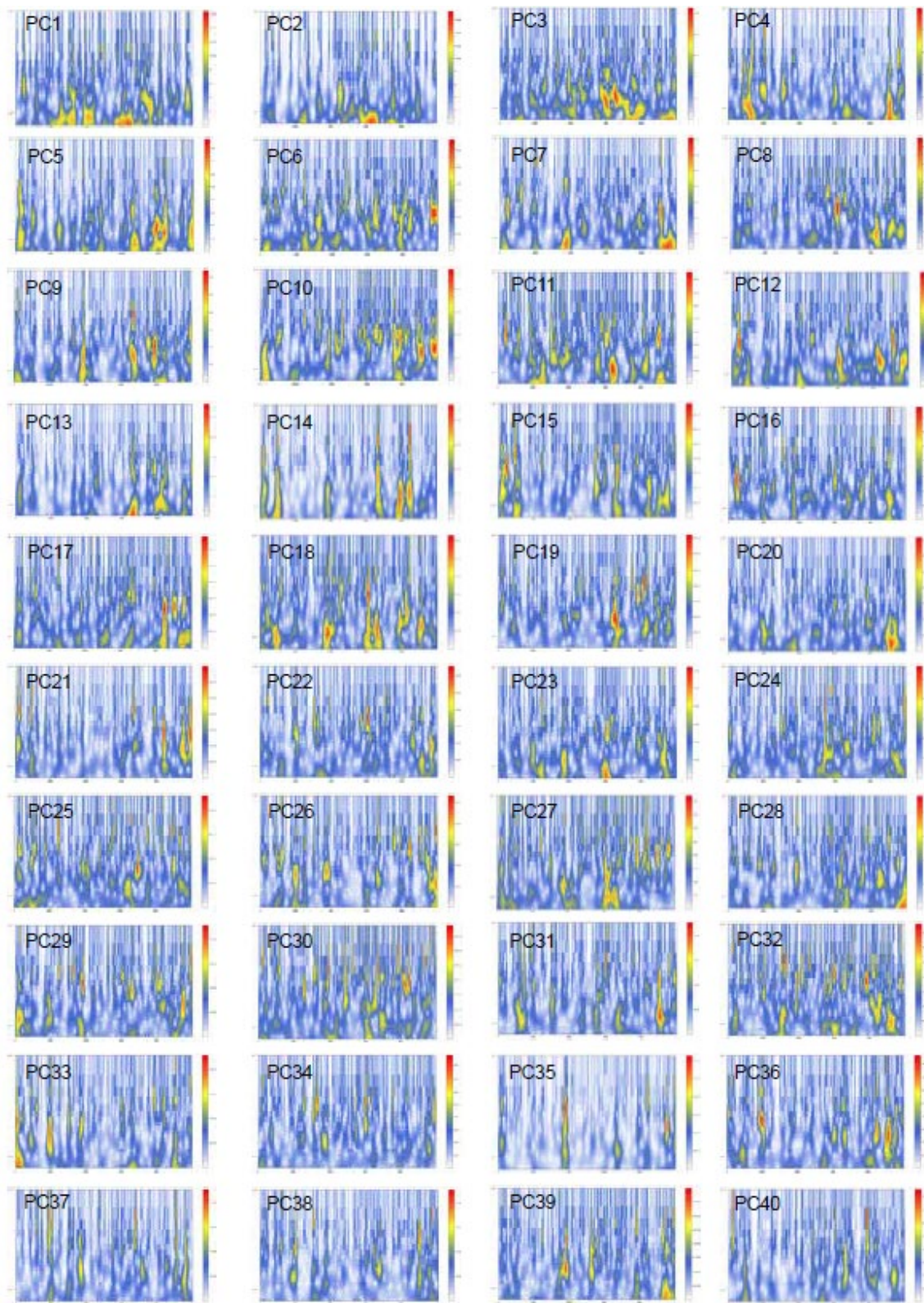
456

457

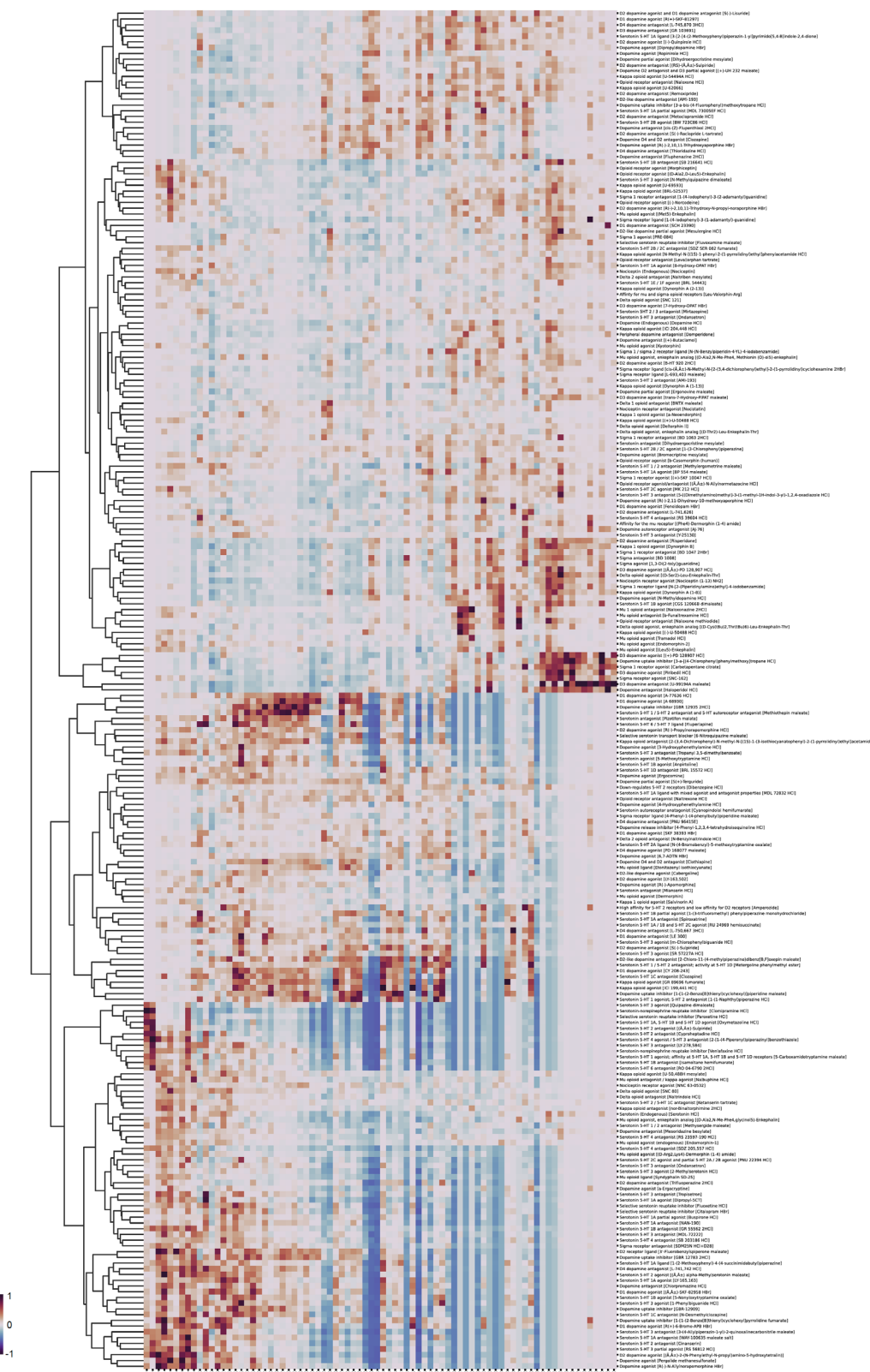
SUPPLEMENTARY DATA



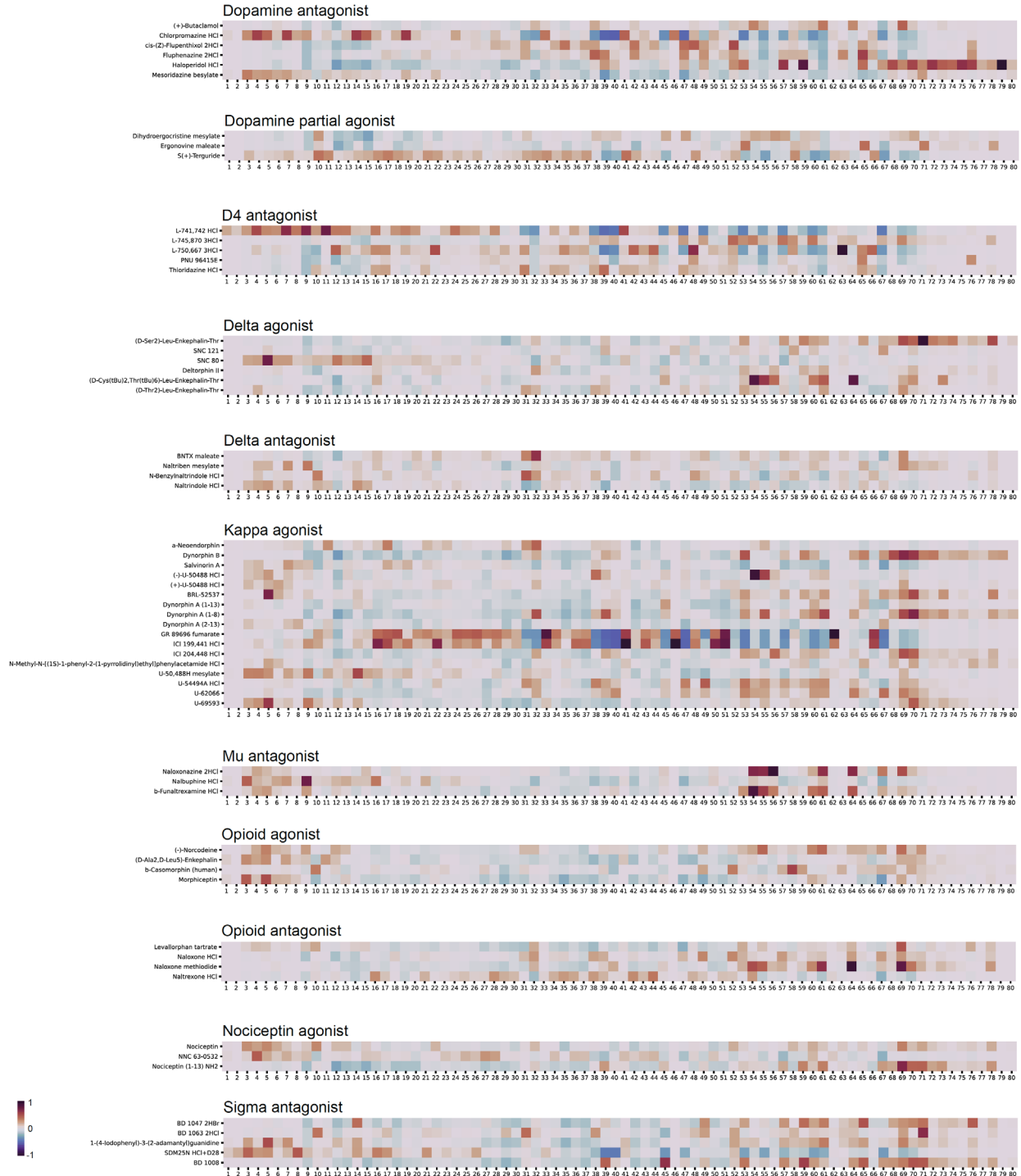
459 **Supplementary Figure 1.** (a) The 3D design of one ZeChat unit. (b) The 3D design of a comb-like insert
460 for blocking the views of fish before ZeChat test. (c) Example preprocessed images. (d) Example input
461 images, latent vectors, and reconstructed images.



463 **Supplementary Figure 2.** An example of spectrograms generated by time-frequency analysis of 40
464 principal components of a latent vector. PC1-40: principal components 1-40. Horizontal axis: frames.
465 Vertical axis: frequencies. Color bar: amplitudes.

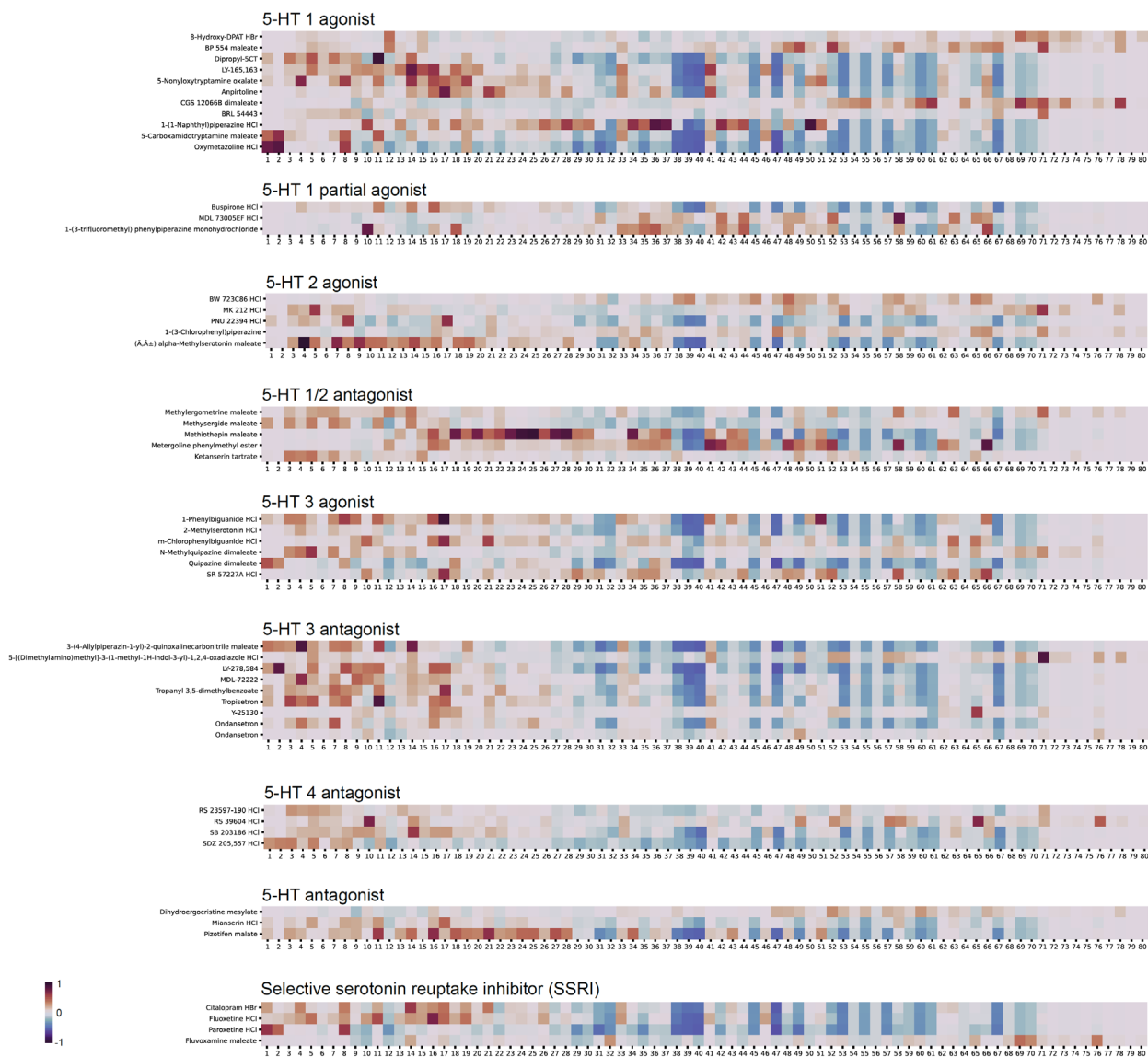


467 **Supplementary Figure 3.** Hierarchical clustering of 237 behavioral fingerprints generated by the screen.
468 The behavioral fingerprints are normalized and subtracted by the median DMSO fingerprint. Labels on the
469 right show: drug classification [drug name].



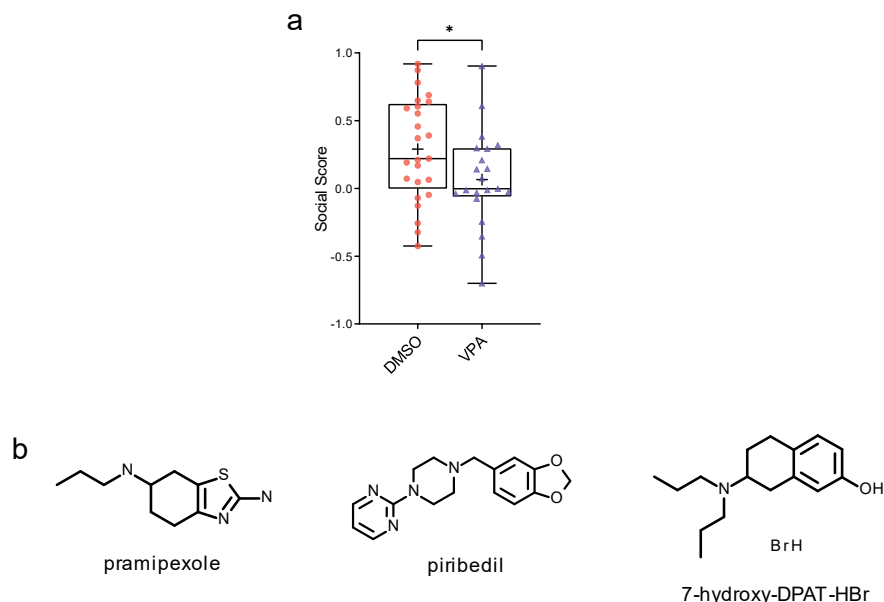
471 **Supplementary Figure 4.** Behavioral fingerprints of dopamine pathway and opioid pathway modulators,
 472 grouped by drug effects.

473



475 **Supplementary Figure 5.** Behavioral fingerprints of serotonin pathway modulators, grouped by drug
476 effects.

477



479 **Supplementary Figure 6. (a)** Boxplot showing social preference (social score) of fish treated by DMSO
480 (n=25) or valproic acid (VPA; n=21) during the first 3 days of embryonic development. *: $p < 0.05$. **(b)**
481 Chemical structures of the D3 agonists pramipexole, piribedil, and 7-hydroxy-DPAT-HBr.

482
483 **Supplementary Video 1.** Video recording of a pair of fish interacting in a ZeChat unit. Each unit is divided
484 into two arenas by a transparent window.

485
486 **Supplementary Video 2.** Video recording of 40 pairs of fish interacting in a full-sized ZeChat test array.

487
488 **Supplementary Video 3.** A combination of 4 processed clips of the same video recording, showing the
489 intermediate and final outcomes of image preprocessing.

490
491 **Supplementary Video 4.** Side-by-side view of fish's behavioral recording and its trajectory on ZeChat
492 map in real-time to visualize how a fish's behavior translates to datapoint embeddings in the ZeChat map.

493
494 **Supplementary Video 5.** Video recordings of wild type (DMSO) and dopamine D3 agonist-treated (10
495 μM piribedil) fish. Demonstrating a more intense interaction pattern between pairs of D3 agonist-treated
496 fish compared to the wild type.

497

498

REFERENCES

- 499 1 Mandell, D. S. *et al.* Psychotropic medication use among Medicaid-enrolled children with autism
500 spectrum disorders. *Pediatrics* **121**, e441-448, doi:10.1542/peds.2007-0984 (2008).
- 501 2 Downs, J. *et al.* Clinical predictors of antipsychotic use in children and adolescents with autism
502 spectrum disorders: a historical open cohort study using electronic health records. *Eur Child*
503 *Adolesc Psychiatry* **25**, 649-658, doi:10.1007/s00787-015-0780-7 (2016).
- 504 3 Geng, Y. & Peterson, R. T. The zebrafish subcortical social brain as a model for studying social
505 behavior disorders. *Dis Model Mech* **12**, doi:10.1242/dmm.039446 (2019).
- 506 4 Kokel, D. *et al.* Rapid behavior-based identification of neuroactive small molecules in the zebrafish.
507 *Nat Chem Biol* **6**, 231-237, doi:10.1038/nchembio.307 (2010).
- 508 5 Bruni, G. *et al.* Zebrafish behavioral profiling identifies multitarget antipsychotic-like compounds.
509 *Nat Chem Biol* **12**, 559-566, doi:10.1038/nchembio.2097 (2016).
- 510 6 Rihel, J. *et al.* Zebrafish behavioral profiling links drugs to biological targets and rest/wake
511 regulation. *Science* **327**, 348-351, doi:10.1126/science.1183090 (2010).
- 512 7 Jordi, J. *et al.* High-throughput screening for selective appetite modulators: A multibehavioral and
513 translational drug discovery strategy. *Sci Adv* **4**, eaav1966, doi:10.1126/sciadv.aav1966 (2018).
- 514 8 Dreosti, E., Lopes, G., Kampff, A. R. & Wilson, S. W. Development of social behavior in young
515 zebrafish. *Front Neural Circuits* **9**, 39, doi:10.3389/fncir.2015.00039 (2015).
- 516 9 Stednitz, S. J. *et al.* Forebrain Control of Behaviorally Driven Social Orienting in Zebrafish. *Curr*
517 *Biol* **28**, 2445-2451 e2443, doi:10.1016/j.cub.2018.06.016 (2018).
- 518 10 Miller, N. & Gerlai, R. Quantification of shoaling behaviour in zebrafish (*Danio rerio*). *Behav Brain*
519 *Res* **184**, 157-166, doi:10.1016/j.bbr.2007.07.007 (2007).
- 520 11 Tang, W. *et al.* Genetic Control of Collective Behavior in Zebrafish. *iScience* **23**, 100942,
521 doi:10.1016/j.isci.2020.100942 (2020).
- 522 12 Berman, G. J., Choi, D. M., Bialek, W. & Shaevitz, J. W. Mapping the stereotyped behaviour of
523 freely moving fruit flies. *J R Soc Interface* **11**, doi:10.1098/rsif.2014.0672 (2014).
- 524 13 Farneback, G. Two-frame motion estimation based on polynomial expansion. *Lect Notes Comput*
525 *Sc* **2749**, 363-370, doi:DOI 10.1007/3-540-45103-x_50 (2003).
- 526 14 Hinton, L. J. P. v. d. M. a. G. E. Visualizing High-Dimensional Data Using t-SNE. *Journal of*
527 *Machine Learning Research* **9**, 2579-2605 (2008).
- 528 15 Andrej Gisbrecht, A. S., Barbara Hammer. Parametric nonlinear dimensionality reduction using
529 kernel t-SNE. *Neurocomputing* **147**, 71-82 (2015).
- 530 16 Gunaydin, L. A. & Deisseroth, K. Dopaminergic Dynamics Contributing to Social Behavior. *Cold*
531 *Spring Harb Symp Quant Biol* **79**, 221-227, doi:10.1101/sqb.2014.79.024711 (2014).
- 532 17 Kiser, D., Steemers, B., Branchi, I. & Homberg, J. R. The reciprocal interaction between serotonin
533 and social behaviour. *Neurosci Biobehav Rev* **36**, 786-798, doi:10.1016/j.neubiorev.2011.12.009
534 (2012).
- 535 18 Pellissier, L. P., Gandia, J., Laboute, T., Becker, J. A. J. & Le Merrer, J. mu opioid receptor, social
536 behaviour and autism spectrum disorder: reward matters. *Br J Pharmacol* **175**, 2750-2769,
537 doi:10.1111/bph.13808 (2018).
- 538 19 Nicolini, C. & Fahnestock, M. The valproic acid-induced rodent model of autism. *Exp Neurol* **299**,
539 217-227, doi:10.1016/j.expneurol.2017.04.017 (2018).
- 540 20 Chen, J. *et al.* Developmental and behavioral alterations in zebrafish embryonically exposed to
541 valproic acid (VPA): An aquatic model for autism. *Neurotoxicol Teratol* **66**, 8-16,
542 doi:10.1016/j.ntt.2018.01.002 (2018).
- 543 21 Geng, Y. *et al.* Top2a promotes the development of social behavior via PRC2 and H3K27me3.
544 *bioRxiv*, doi:10.1101/2021.09.20.461107 (2021).
- 545 22 Branson, K., Robie, A. A., Bender, J., Perona, P. & Dickinson, M. H. High-throughput ethomics in
546 large groups of *Drosophila*. *Nat Methods* **6**, 451-457, doi:10.1038/nmeth.1328 (2009).
- 547 23 Dankert, H., Wang, L., Hoopfer, E. D., Anderson, D. J. & Perona, P. Automated monitoring and

- 548 analysis of social behavior in *Drosophila*. *Nat Methods* **6**, 297-303, doi:10.1038/nmeth.1310 (2009).
- 549 24 Laan, A., Iglesias-Julios, M. & de Polavieja, G. G. Zebrafish aggression on the sub-second time
550 scale: evidence for mutual motor coordination and multi-functional attack manoeuvres. *R Soc Open*
551 *Sci* **5**, 180679, doi:10.1098/rsos.180679 (2018).
- 552 25 Hong, W. *et al.* Automated measurement of mouse social behaviors using depth sensing, video
553 tracking, and machine learning. *Proc Natl Acad Sci U S A* **112**, E5351-5360,
554 doi:10.1073/pnas.1515982112 (2015).
- 555 26 de Chaumont, F. *et al.* Computerized video analysis of social interactions in mice. *Nat Methods* **9**,
556 410-417, doi:10.1038/nmeth.1924 (2012).
- 557 27 Harpaz, R., Tkacik, G. & Schneidman, E. Discrete modes of social information processing predict
558 individual behavior of fish in a group. *Proc Natl Acad Sci U S A* **114**, 10149-10154,
559 doi:10.1073/pnas.1703817114 (2017).
- 560 28 Brown, A. E., Yemini, E. I., Grundy, L. J., Jucikas, T. & Schafer, W. R. A dictionary of behavioral
561 motifs reveals clusters of genes affecting *Caenorhabditis elegans* locomotion. *Proc Natl Acad Sci*
562 *U S A* **110**, 791-796, doi:10.1073/pnas.1211447110 (2013).
- 563 29 Stephens, G. J., Bueno de Mesquita, M., Ryu, W. S. & Bialek, W. Emergence of long timescales
564 and stereotyped behaviors in *Caenorhabditis elegans*. *Proc Natl Acad Sci U S A* **108**, 7286-7289,
565 doi:10.1073/pnas.1007868108 (2011).
- 566 30 Costa, A. C., Ahamed, T. & Stephens, G. J. Adaptive, locally linear models of complex dynamics.
567 *Proc Natl Acad Sci U S A* **116**, 1501-1510, doi:10.1073/pnas.1813476116 (2019).
- 568 31 Stephens, G. J., Johnson-Kerner, B., Bialek, W. & Ryu, W. S. Dimensionality and dynamics in the
569 behavior of *C. elegans*. *PLoS Comput Biol* **4**, e1000028, doi:10.1371/journal.pcbi.1000028 (2008).
- 570 32 Broekmans, O. D., Rodgers, J. B., Ryu, W. S. & Stephens, G. J. Resolving coiled shapes reveals
571 new reorientation behaviors in *C. elegans*. *Elife* **5**, doi:10.7554/eLife.17227 (2016).
- 572 33 Gomez-Marin, A., Stephens, G. J. & Brown, A. E. Hierarchical compression of *Caenorhabditis*
573 *elegans* locomotion reveals phenotypic differences in the organization of behaviour. *J R Soc*
574 *Interface* **13**, doi:10.1098/rsif.2016.0466 (2016).
- 575 34 Szigeti, B., Deogade, A. & Webb, B. Searching for motifs in the behaviour of larval *Drosophila*
576 *melanogaster* and *Caenorhabditis elegans* reveals continuity between behavioural states. *J R Soc*
577 *Interface* **12**, 20150899, doi:10.1098/rsif.2015.0899 (2015).
- 578 35 Berman, G. J., Bialek, W. & Shaevitz, J. W. Predictability and hierarchy in *Drosophila* behavior.
579 *Proc Natl Acad Sci U S A* **113**, 11943-11948, doi:10.1073/pnas.1607601113 (2016).
- 580 36 Todd, J. G., Kain, J. S. & de Bivort, B. L. Systematic exploration of unsupervised methods for
581 mapping behavior. *Phys Biol* **14**, 015002, doi:10.1088/1478-3975/14/1/015002 (2017).
- 582 37 DeAngelis, B. D., Zavatone-Veth, J. A. & Clark, D. A. The manifold structure of limb coordination
583 in walking *Drosophila*. *Elife* **8**, doi:10.7554/eLife.46409 (2019).
- 584 38 Pereira, T. D. *et al.* Fast animal pose estimation using deep neural networks. *Nat Methods* **16**, 117-
585 125, doi:10.1038/s41592-018-0234-5 (2019).
- 586 39 Cande, J. *et al.* Optogenetic dissection of descending behavioral control in *Drosophila*. *Elife* **7**,
587 doi:10.7554/eLife.34275 (2018).
- 588 40 Marques, J. C., Lackner, S., Felix, R. & Orger, M. B. Structure of the Zebrafish Locomotor
589 Repertoire Revealed with Unsupervised Behavioral Clustering. *Curr Biol* **28**, 181-195 e185,
590 doi:10.1016/j.cub.2017.12.002 (2018).
- 591 41 Mearns, D. S., Donovan, J. C., Fernandes, A. M., Semmelhack, J. L. & Baier, H. Deconstructing
592 Hunting Behavior Reveals a Tightly Coupled Stimulus-Response Loop. *Curr Biol* **30**, 54-69 e59,
593 doi:10.1016/j.cub.2019.11.022 (2020).
- 594 42 Semmelhack, J. L. *et al.* A dedicated visual pathway for prey detection in larval zebrafish. *Elife* **3**,
595 doi:10.7554/eLife.04878 (2014).
- 596 43 Wiltshcko, A. B. *et al.* Mapping Sub-Second Structure in Mouse Behavior. *Neuron* **88**, 1121-1135,
597 doi:10.1016/j.neuron.2015.11.031 (2015).
- 598 44 Markowitz, J. E. *et al.* The Striatum Organizes 3D Behavior via Moment-to-Moment Action

599 Selection. *Cell* **174**, 44-58 e17, doi:10.1016/j.cell.2018.04.019 (2018).
600 45 Klibaite, U., Berman, G. J., Cande, J., Stern, D. L. & Shaevitz, J. W. An unsupervised method for
601 quantifying the behavior of paired animals. *Phys Biol* **14**, 015006, doi:10.1088/1478-3975/aa5c50
602 (2017).
603 46 Klibaite, U. & Shaevitz, J. W. Paired fruit flies synchronize behavior: Uncovering social
604 interactions in *Drosophila melanogaster*. *PLoS Comput Biol* **16**, e1008230,
605 doi:10.1371/journal.pcbi.1008230 (2020).
606 47 Romero-Ferrero, F., Bergomi, M. G., Hinz, R. C., Heras, F. J. H. & de Polavieja, G. G. idtracker.ai:
607 tracking all individuals in small or large collectives of unmarked animals. *Nat Methods*,
608 doi:10.1038/s41592-018-0295-5 (2019).
609 48 Shuo Hong Wang, J. Z., Xiang Liu, Zhi-Ming Qian, Ye Liu, Yan Qiu Chen. 3D tracking
610 swimming fish school with learned kinematic model using LSTM network. *IEEE International*
611 *Conference on Acoustics, Speech and Signal Processing (ICASSP)*,
612 doi:10.1109/ICASSP.2017.7952320 (2017).
613 49 Heras, F. J. H., Romero-Ferrero, F., Hinz, R. C. & de Polavieja, G. G. Deep attention networks
614 reveal the rules of collective motion in zebrafish. *PLoS Comput Biol* **15**, e1007354,
615 doi:10.1371/journal.pcbi.1007354 (2019).
616 50 Hood, S. D. *et al.* Dopaminergic challenges in social anxiety disorder: evidence for dopamine D3
617 desensitisation following successful treatment with serotonergic antidepressants. *J*
618 *Psychopharmacol* **24**, 709-716, doi:10.1177/0269881108098144 (2010).
619 51 Kagaya, T. *et al.* Dopamine D3 agonists disrupt social behavior in rats. *Brain Res* **721**, 229-232,
620 doi:10.1016/0006-8993(96)00288-0 (1996).
621 52 Gendreau, P. L., Petitto, J. M., Petrova, A., Garipey, J. & Lewis, M. H. D(3) and D(2) dopamine
622 receptor agonists differentially modulate isolation-induced social-emotional reactivity in mice.
623 *Behav Brain Res* **114**, 107-117, doi:10.1016/s0166-4328(00)00193-5 (2000).
624 53 Hoffman, E. J. *et al.* Estrogens Suppress a Behavioral Phenotype in Zebrafish Mutants of the
625 Autism Risk Gene, CNTNAP2. *Neuron* **89**, 725-733, doi:10.1016/j.neuron.2015.12.039 (2016).
626 54 Mwaffo, V., Zhang, P., Romero Cruz, S. & Porfiri, M. Zebrafish swimming in the flow: a particle
627 image velocimetry study. *PeerJ* **5**, e4041, doi:10.7717/peerj.4041 (2017).
628 55 Lopes, G. *et al.* Bonsai: an event-based framework for processing and controlling data streams.
629 *Front Neuroinform* **9**, 7, doi:10.3389/fninf.2015.00007 (2015).
630 56 Zivkovic, Z. & van der Heijden, F. Efficient adaptive density estimation per image pixel for the
631 task of background subtraction. *Pattern Recogn Lett* **27**, 773-780, doi:10.1016/j.patrec.2005.11.005
632 (2006).
633